Balanced Micro/Macro Contact Model for Forward Dynamics of Rigid Multibody

Tomomichi Sugihara and Yoshihiko Nakamura
Department of Mechano-informatics, Graduate school of University of Tokyo
7–3–1, Hongo, Bunkyo-ku, Tokyo, Japan
sugihara@ynl.t.u-tokyo.ac.jp

***Abstract*— This paper proposes a computational method of contact forces working between multibody system and environment in forward dynamics based on both the micro-body-deformation model and macro contact model. The combination of them simultaneously prevents the simulation from excess penetration in micro contact model and chattering in macro contact model. The difficulty lies on how to absorb the difference of duration between them. This problem is solved through the introduction of a timestep-dependent variable damper for a micro contact model and of error-norm minimization for a macro contact model.**

***Index Terms*— Multibody forward dynamics, Collision and contact force, Dynamics simulation**

I. Introduction

As well as the robot dynamics model, the contact model with the environment is a key to gain reliable results in forward dynamics of robot motions with frequent collision such as contouring control or legged control. The conventional contact models are classified into the following *micro contact model* and *macro contact model*.

Micro contact model is of tiny elastic deformations of colliding bodies. It computes the acting forces in accordance with only the local relative movements of those bodies, so that it facilitates implementations. Deformations of bodies in a micro level, however, happen in quite a shorter time than the movements of bodies. Consequently, microsecond order's integration time step is required for the forward dynamics simulation, while millisecond order's is for the ordinary multibody dynamics computation. Otherwise, the integration likely diverges. Moreover, it is impossible in principle to compute static friction force. Poisson's model [1], linear spring-damper model [2] [3] [4], non-linear spring-damper model [5] [6] have been proposed as this class. Macro contact model approximates the collision as a macro-scale phenomenon based on the momentum conservation law, regarding the environment as a rigid object. It inversely computes the impulse exerted to the bodies from the difference of the velocity immediately before and after collision, taking rebound coefficient and friction into account. It is numerically stable since it directly calculates a discontinuous change of velocity, while micro model does continuous change of acceleration. However, chattering at the contact points easily happens. And, hyperstatistics problem also arises. Computation of forces by quadratic programming [7] [8] [9], and by a successive modification of supposed contact condition and constraints at each contact point [4] have been proposed as this class.

This paper describes an unification of those models in the forward dynamics simulation for the following two purposes. One is to enable to compose the environment model by materials with rich properties. The other is to avoid both excess penetration of the collision points in micro contact model and chuttering in macro model simultaneously by covering rigid bodies with thin elastic membrane. Coexistence of those models, which in nature happen in different durations, in the same integration time step is achieved by the use of a similar technique to of Yamane et al.'s[4]. And, friction force is strictly computed in macro contact model. Fujimoto et al.'s method[9] cannot compute static friction force. Son et al.[10] approximately linearized the friction cone to be easily handled by substituting it with the polygonal pyramid, which requires a large increase of computation cost in order to improve accuracy.

II. Multilink system and contact model

A. Equation of motion

Suppose that any contact situations are represented by points which the colliding edges and faces consist of, so that only a linear force works at each point. The equation of motion of an open-chain system which interacts with the environment generally forms as the following equation.

$$\boldsymbol{H}\ddot{\boldsymbol{q}} + \boldsymbol{b} = \boldsymbol{u} + \sum_{i\in\mathcal{C}} \boldsymbol{K}_i \boldsymbol{f}_i \tag{1}$$

$$\boldsymbol{b} \equiv \dot{\boldsymbol{H}}\dot{\boldsymbol{q}} + \hat{\boldsymbol{b}} \tag{2}$$

where $\boldsymbol{H}$ is the inertia matrix, $\boldsymbol{q}$ is the generalized coordinates, $\boldsymbol{b}$ is the non-linear bias force including centrifugal-Coriolis-gravity forces, $\hat{\boldsymbol{b}}$ is the gravity force, $\boldsymbol{u}$ is the generalized force, $\mathcal{C}$ is the set of indices of the whole contact points, $\boldsymbol{f}_i$ is the linear force acting at ith contact point and $\boldsymbol{K}_i$ is the Jacobian transpose defined by the following equation for the contact point $\boldsymbol{p}_i$ where $\boldsymbol{f}_i$ acts.

$$\boldsymbol{K}_i = \left(\frac{\partial \boldsymbol{p}_i}{\partial \boldsymbol{q}}\right)^T \tag{3}$$

$\boldsymbol{H}$, $\boldsymbol{b}$ and $\boldsymbol{K}_i$ are obtained by Walker and Orin's [11]. When $\boldsymbol{u}$ is given and $\boldsymbol{f}_i$ is calculated by any means, $\ddot{\boldsymbol{q}}$ is obtained from Eq.(1). Forward dynamics simulation is achieved by integrating it and updating $\dot{\boldsymbol{q}}$ and $\boldsymbol{q}$.

B. Contact point motion and friction

Suppose P is a corresponding face to a contact point $\boldsymbol{p}_i$. P is on the model of environment for $\boldsymbol{p}_i$ on the links, or the contrary. Suppose $\boldsymbol{p}_E$ is a point on P and $\boldsymbol{\nu}_i$ is the unit normal vector of P, the penetration depth d_i of $\boldsymbol{p}_i$ into P is calculated from Eq.(4).

$$d_i = -\boldsymbol{\nu}_i^T(\boldsymbol{p}_i - \boldsymbol{p}_E) \tag{4}$$

The velocity of $\boldsymbol{p}_i$, $\boldsymbol{v}_i \equiv \dot{\boldsymbol{p}}_i$ is decomposed into the normal component to the face and the parallel component (the slip velocity) as Fig. 1 shows.

$$\boldsymbol{v}_i = v_{\nu i}\boldsymbol{\nu}_i + \boldsymbol{v}_{\sigma i} \tag{5}$$

where $v_{\nu i} \equiv -\dot{d}_i = \boldsymbol{\nu}_i^T\boldsymbol{v}_i$, and $\boldsymbol{v}_{\sigma i}$ satisfies the following.

$$\boldsymbol{\nu}_i^T\boldsymbol{v}_{\sigma i} = 0 \tag{6}$$

Let us define the slip vector $\boldsymbol{\sigma}_i$ as:

$$\boldsymbol{\sigma}_i \equiv \begin{cases} \dfrac{\boldsymbol{v}_{\sigma i}}{v_{\sigma i}} & (v_{\sigma i} > \varepsilon) \\ \boldsymbol{0} & (v_{\sigma i} \leq \varepsilon) \end{cases} \tag{7}$$

where ε is a tiny value, and $v_{\sigma i}$ is defined as:

$$v_{\sigma i} \equiv \| \boldsymbol{v}_{\sigma i} \| = \| \boldsymbol{v}_i - v_{\nu i}\boldsymbol{\nu}_i \| \tag{8}$$

The external force $\boldsymbol{f}_i$ is also decomposed into the normal force $f_{\nu i}$ and the friction force $\boldsymbol{f}_{\phi i}$ as follows.

$$\boldsymbol{f}_i = f_{\nu i}\boldsymbol{\nu}_i + \boldsymbol{f}_{\phi i} \tag{9}$$

where $f_{\nu i} \equiv \boldsymbol{\nu}_i^T\boldsymbol{f}_i$, and $\boldsymbol{f}_{\phi i}$ satisfies the following.

$$\boldsymbol{\nu}_i^T\boldsymbol{f}_{\phi i} = 0 \tag{10}$$

When $v_{\sigma i} > \varepsilon$, a kinetic friction force represented by the following equation works at $\boldsymbol{p}_i$.

$$\boldsymbol{f}_{\phi i} = -\mu_{Ki}f_{\nu i}\boldsymbol{\sigma}_i \tag{11}$$

where μ_{Ki} is the kinetic friction coefficient. From Eq.(9):

$$\boldsymbol{f}_i = f_{\nu i}(\boldsymbol{\nu}_i - \mu_{Ki}\boldsymbol{\sigma}_i) \tag{12}$$

In this case, the direction of the force is known, while the magnitude of it is unknown. And when $v_{\sigma i} \leq \varepsilon$, a static force works at $\boldsymbol{p}_i$, and $\boldsymbol{f}_{\phi i}$ constrains $\boldsymbol{p}_i$ so long as it is less than the maximum static friction force. In this case, neither the direction nor the magnitude is known.

III. Unification of micro/macro contact model

A. Micro contact model with timestep-dependent damper

Here, we adopt linear spring-damper model as micro contact model. Numerical divergence in the model is due to the following reason. Suppose the contact is modeled by a spring coefficient k_i and a damping coefficient c_i, the reaction force $f_{\nu i}$ is ordinarily calculated as follows.

$$f_{\nu i} = \begin{cases} -k_i d_i - c_i\dot{d}_i & (\text{if} \quad \dot{d}_i > 0) \\ -k_i d_i & (\text{otherwise}) \end{cases} \tag{13}$$

And the assumption that d_i varies $\Delta d_i \simeq \dot{d}_i\Delta t$ during the time step Δt implies that the force is estimated by the minimum value in compression phase, and by the maximum value in restitution phase as figured in Fig.2. This encourages deeper penetration of the contact point into the environment, causing the excess accumulation of strain energy and stronger rebound. Joukhadar et al.[12] proposed an adaptive modification of Δt to subdue the variation of kinetic energy within a certain amount, which requires recomputation in each step, so that it is time-consuming. Here, we propose to use the following equation instead of Eq.(13) in order to prevent such numerical phenomena.

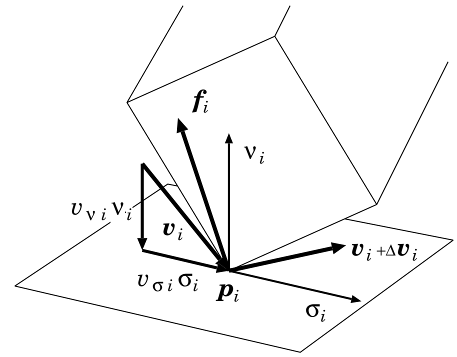

Fig. 1. Contact point, velocity and force

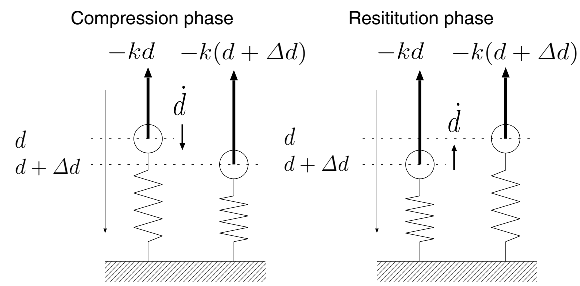

Fig. 2. Elastic force estimation in numerical integration

$$f_{\nu i} = \begin{cases} -k_i(d_i + \dot{d}_i\Delta t) - c_i\dot{d}_i & (\text{if} \quad \dot{d}_i > 0) \\ -k_i(d_i + \dot{d}_i\Delta t) & (\text{otherwise}) \end{cases} \tag{14}$$

It effects oppositely against the ordinary method, namely, the penetration in compression phase is lessen and the rebound in restitution phase is weaken. This is in principle based on the same idea with implicit integration introduced in [4]. Incidentally, Eq.(14) is rewrote as follows.

$$f_{\nu i} = \begin{cases} -k_i d_i - (c_i + k_i\Delta t)\dot{d}_i & (\text{if} \quad \dot{d}_i > 0) \\ -k_i d_i - k_i\Delta t\dot{d}_i & (\text{otherwise}\dot{d}_i \leq 0) \end{cases} \tag{15}$$

One can interpret it as the damping coefficient adaptively varies depending on Δt. It is substitutable with nonlinear spring model[5] or Poisson's model[1] since the restitution force monotonously increases as the point penetrates more deeply. $\boldsymbol{f}_i$ is obtained from Eq.(14), (7) and (12).

B. Macro contact model with error-norm minimization

Here, we group the contact points to ones based on micro contact model $\{\boldsymbol{P}_i | i \in \mathcal{T}\}$ and on macro contact model $\{\boldsymbol{P}_i | i \in \mathcal{H}\}$. Then, Eq.(1) becomes as follows.

$$\boldsymbol{H}\ddot{\boldsymbol{q}} + \boldsymbol{b} = \boldsymbol{u} + \sum_{i\in\mathcal{H}}\boldsymbol{K}_i\boldsymbol{f}_i + \sum_{i\in\mathcal{T}}\boldsymbol{K}_i\boldsymbol{f}_i \tag{16}$$

Since micro contact force is obtained in advance from Eq.(14), Eq.(16) can be rewritten as follows.

$$\boldsymbol{H}\ddot{\boldsymbol{q}} + \boldsymbol{b} = \boldsymbol{u}_E + \sum_{i \in \mathcal{H}} \boldsymbol{K}_i \boldsymbol{f}_i \tag{17}$$

$$\boldsymbol{u}_E \equiv \boldsymbol{u} + \sum_{i \in \mathcal{T}} \boldsymbol{K}_i \boldsymbol{f}_i \tag{18}$$

Let us assume that the variations of $\boldsymbol{H}$, $\boldsymbol{b}$, $\boldsymbol{u}_E$ and $\boldsymbol{K}_i$ during Δt are ignorable. Suppose $\boldsymbol{v}_i$ and $\dot{\boldsymbol{q}}$ change in Δt to $\boldsymbol{v}_i + \Delta\boldsymbol{v}_i$ and $\dot{\boldsymbol{q}} + \Delta\dot{\boldsymbol{q}}$, respectively. From Eq.(3), one can derive the following equation.

$$\boldsymbol{K}_i^T \Delta\dot{\boldsymbol{q}} = \Delta\boldsymbol{v}_i \qquad (i \in \mathcal{H}) \tag{19}$$

And, integrating Eq.(17) by Δt, we get:

$$\boldsymbol{H}\Delta\dot{\boldsymbol{q}} = \int_{\Delta t} (\boldsymbol{u}_E - \hat{\boldsymbol{b}} + \sum_{i \in \mathcal{H}} \boldsymbol{K}_i \boldsymbol{f}_i)\, dt = \Delta\hat{\boldsymbol{u}} + \sum_{i \in \mathcal{H}} \boldsymbol{K}_i \Delta\boldsymbol{f}_i \tag{20}$$

$$\Delta\hat{\boldsymbol{u}} \equiv \int_{\Delta t} (\boldsymbol{u}_E - \hat{\boldsymbol{b}})\, dt \simeq (\boldsymbol{u}_E - \hat{\boldsymbol{b}})\Delta t \tag{21}$$

$$\Delta\boldsymbol{f}_i \equiv \int_{\Delta t} \boldsymbol{f}_i\, dt \tag{22}$$

From Eq.(19) and (20), the following equation is derived.

$$\boldsymbol{K}_i^T \boldsymbol{H}^{-1} \sum_{j \in \mathcal{H}} \boldsymbol{K}_j \Delta\boldsymbol{f}_j = \Delta\boldsymbol{v}_i - \boldsymbol{v}_{Bi} \tag{23}$$

$$\boldsymbol{v}_{Bi} \equiv \boldsymbol{K}_i^T \boldsymbol{H}^{-1} \Delta\hat{\boldsymbol{u}} \tag{24}$$

In the case that $\boldsymbol{p}_i$ is not moving (i.e. $\| \boldsymbol{v}_i \| \leq \varepsilon$), a static friction force acts at $\boldsymbol{p}_i$ to remain the point stationary.

$$\boldsymbol{v}_i + \Delta\boldsymbol{v}_i = \boldsymbol{0}. \tag{25}$$

And, neither the magnitude nor the direction of $\Delta\boldsymbol{f}_i$ is known. When $\| \boldsymbol{v}_i \| > \varepsilon$, a kinetic friction force acts at $\boldsymbol{p}_i$. From Eq.(12), $\Delta\boldsymbol{f}_i$ is represented as follows.

$$\Delta\boldsymbol{f}_i = \Delta f_{\nu i}(\boldsymbol{\nu}_i - \mu_{Ki}\boldsymbol{\sigma}_i) \tag{26}$$

And $\Delta\boldsymbol{v}_i$ is decomposed as follows.

$$\Delta\boldsymbol{v}_i = \Delta v_{\nu i}\boldsymbol{\nu}_i + \Delta\boldsymbol{v}_{\sigma_i} \tag{27}$$

where

$$\Delta v_{\nu i} = \boldsymbol{\nu}_i^T \Delta\boldsymbol{v}_i, \quad \boldsymbol{\nu}_i^T \Delta\boldsymbol{v}_{\sigma i} = 0 \tag{28}$$

Let e_i be the rebound coefficient at $\boldsymbol{p}_i$, we get:

$$\Delta v_{\nu i} = -(1 + e_i) v_{\nu i} \tag{29}$$

And, $\Delta\boldsymbol{v}_{\sigma_i}$ is unknown.

Suppose $\mathcal{S}$ and $\mathcal{K}$ are the set of point indices i at which the static friction force and the kinetic friction force work, respectively. Now, we conclude as follows from Eq.(23), (25), (26), (27), (28) and (29).

$$\boldsymbol{K}_i^T \boldsymbol{H}^{-1} \left\{ \sum_{j \in \mathcal{S}} \boldsymbol{K}_j \Delta\boldsymbol{f}_j + \sum_{j \in \mathcal{K}} \Delta f_{\nu j} \boldsymbol{K}_j (\boldsymbol{\nu}_j - \mu_{Kj}\boldsymbol{\sigma}_j) \right\} = -\boldsymbol{v}_i - \boldsymbol{v}_{Bi} \qquad (\text{for} \quad i \in \mathcal{S}) \tag{30}$$

$$\boldsymbol{\nu}_i^T \boldsymbol{K}_i^T \boldsymbol{H}^{-1} \left\{ \sum_{j \in \mathcal{S}} \boldsymbol{K}_j \Delta\boldsymbol{f}_j + \sum_{j \in \mathcal{K}} \Delta f_{\nu j} \boldsymbol{K}_j (\boldsymbol{\nu}_j - \mu_{Kj}\boldsymbol{\sigma}_j) \right\} = -(1 + e_i) v_{\nu i} - \boldsymbol{\nu}_i^T \boldsymbol{v}_{Bi} \qquad (\text{for} \quad i \in \mathcal{K}) \tag{31}$$

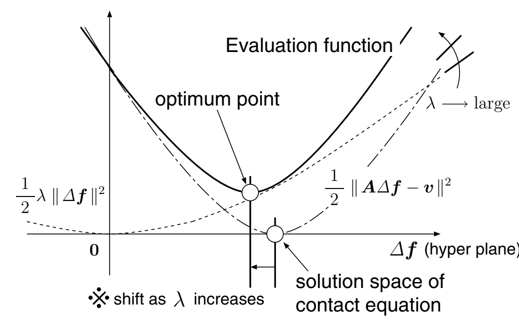

Fig. 3. Relationship between λ and evaluation function in Eq.(33)

Or,

$$\boldsymbol{A}\Delta\boldsymbol{f} = \boldsymbol{v} \tag{32}$$

where $\boldsymbol{A}$ is a positive semidefinite square matrix. If more than three vertices on a link are in contact, $\boldsymbol{A}$ becomes a singular matrix and the problem of hyperstatistics arises, namely, $\Delta\boldsymbol{f}$ is not determined uniquely. And, numerical error incidentally leads to the impossible problem. These factors leave Eq.(32) from the strict solution. Then, we calculate $\Delta\boldsymbol{f}$ by solving the following quadratic programming in order to minimize the residual error of both sides of Eq.(32) and the norm of $\Delta\boldsymbol{f}$ simultaneously.

$$\frac{1}{2} \| \boldsymbol{A}\Delta\boldsymbol{f} - \boldsymbol{v} \|^2 + \frac{1}{2}\lambda \| \Delta\boldsymbol{f} \|^2 \longrightarrow minimize. \quad \text{subject to} \quad \boldsymbol{\nu}_i^T \Delta\boldsymbol{f}_i \geq 0 \quad (i \in \mathcal{H}) \tag{33}$$

where λ is a tiny value. It involves that micro deformation converges in infinitely short term and the strain energy of the bodies becomes almost stationary at any instance. And, the inequality constraint implies that pulling forces cannot work at any contact points. Note that the external force computed by (33) is away from the solution space of Eq.(32) for excess λ (refer to Fig. 3). Averaging $\Delta\boldsymbol{f}_i$ per Δt, $\boldsymbol{f}_i$ is computed as follows.

$$\boldsymbol{f}_i = \frac{\Delta\boldsymbol{f}_i}{\Delta t} \tag{34}$$

C. Modification of friction force

The force computed from (33) and (34) ideally remains the contact points stationary with static friction force. If it exceeds the maximum static friction force, it should shift discontinuously to the kinetic friction force, and, the point will begin to slip. This mechanism is realized by the following procedure. Firstly, we decompose the tentative $\boldsymbol{f}_i$ into $f_{\nu i}$ and $f_{\phi i}$ from Eq.(9), where

$$f_{\phi i} = \| \boldsymbol{f}_{\phi i} \| \tag{35}$$

Let μ_{Si} be the maximum static friction coefficient at $\boldsymbol{p}_i$. As long as $f_{\phi i} \leq \mu_{Si} f_{\nu i}$ is satisfied, a static friction force works, so that it has no inconsistency. If $f_{\phi i} > \mu_{Si} f_{\nu i}$, $\boldsymbol{p}_i$ will slip on the face. In this case, $f_{\phi i}$ is replaced with the kinetic friction force as:

$$f_{\phi i} = \mu_{Ki} f_{\nu i} \tag{36}$$

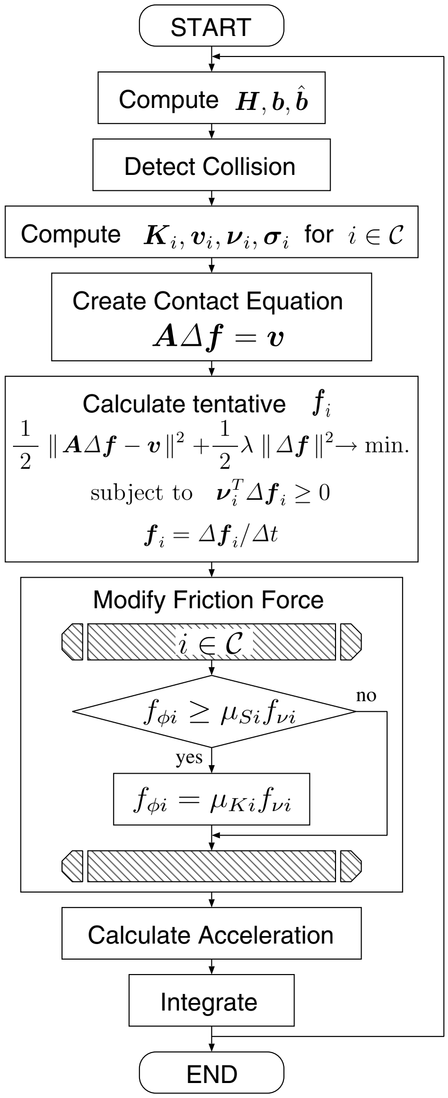

Fig. 4. Flowchart of forward dynamics

D. Procedure of forward dynamics computation

This section shows the complete procedure of forward dynamics including a computation of contact forces.

1) Compute $\boldsymbol{H}$, $\boldsymbol{b}$ and $\hat{\boldsymbol{b}}$.
2) Detect collisions between the multibody system and the environment, and store the set of contact points.
3) For each $\boldsymbol{p}_i$, compute $\boldsymbol{v}_i$, $\boldsymbol{\nu}_i$, $\boldsymbol{\sigma}_i$ and $\boldsymbol{K}_i$.
4) Compute the micro contact forces from Eq.(14), (7) and (12).
5) Create Eq.(32) from Eq.(30), (31) and $\boldsymbol{u}$ in accordance with the macro contact model.
6) Calculate a tentative $\boldsymbol{f}_i$ from (33) and (34).
7) Modify the friction force working at each $\boldsymbol{p}_i$.
8) Calculate $\ddot{\boldsymbol{q}}$ from Eq.(1).
9) Integrate $\ddot{\boldsymbol{q}}$, and update $\dot{\boldsymbol{q}}$ and $\boldsymbol{q}$.

Fig. 4 shows the flowchart. Although the total complexity of computation largely depends on the solution of quadratic programming and thus is hardly estimated, the cost for checking of contact state and of dynamical validity is reduced against the method in [4].

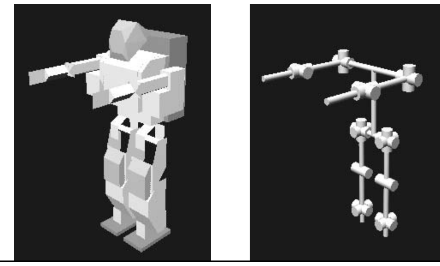

Number of joints:	20 (8 for arms, 12 for legs)
height:	480 [mm]
weight:	5 [kg]

Fig. 5. Geometry, size and mass and joint assignment of the robot

IV. SIMULATION

A. Robot and environment model

The performance of proposed is verified through some simulations with a model of HOAP-1[13]. Fig. 5 shows its geometry and joint assignment. the first order symplectic method was adopted for numerical integration of all the following simulations. They run on a PC with Celeron 2.0GHz and 512MB RAM. The mean computation time for one cycle was about 1.5[ms].

B. Examination of micro contact model

To estimate the power of proposed micro contact model in section III-A, comparing with a conventional, a dropping down of the robot from the height 0.05[m] was simulated. The spring and damping coefficients of the floor were set for 4410[N/m] and 282[N/m·s^{-1}], respectively. Kinetic friction coefficient between the robot and the floor was 0.4. Though both showed numerically stable result for $\Delta t = 0.001$[s], the conventional model unnaturally accelerated the robot after the touchdown onto the floor to leap for $\Delta t = 0.0025$[s] (Fig. 6(C)), while the proposed keeps the robot stable on the floor (Fig. 6(D)).

The excess external force of micro contact model is caused by burst of the number of contact points. Although the proposed suppresses energy exerted from the environment to reduce the risk of numerical divergence, this inherent issue of the model cannot be resolved.

C. Examination of error-norm minimization

The effect of λ introduced in section III-B is examined. The floor was modeled as a rigid body with rebound coefficient 0, maximum static friction coefficient 1.0 and kinetic friction coefficient 0.4. It is covered by a 0.0005[m] elastic membrane with spring coefficient 5512[N/m], damping coefficient 158[N/m·s^{-1}] and kinetic friction coefficient 0.4. Δt was 0.001[s]. $\lambda = 0.01, 0.1, 1.0, 4.0$ were tested for (33), and the standing motion of the robot were simulated for each case. The normal reaction force acting to one of the vertices of the left sole was plotted in Fig. 7. Note that the vertical scale differs from case to case. The external force by macro contact model showed an impulsive behavior for small λ due to chatterings. As λ increases, the external force is smoothed to be closed to realistic behavior. Going on this test, the robot penetrated into the floor due

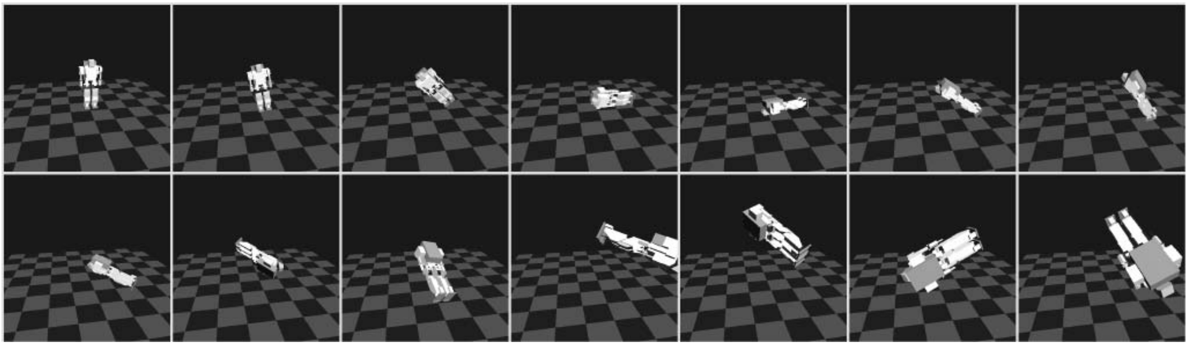

(A) $\Delta t = 0.0025$[s], compute microscopic deformation by conventional Eq.(13)

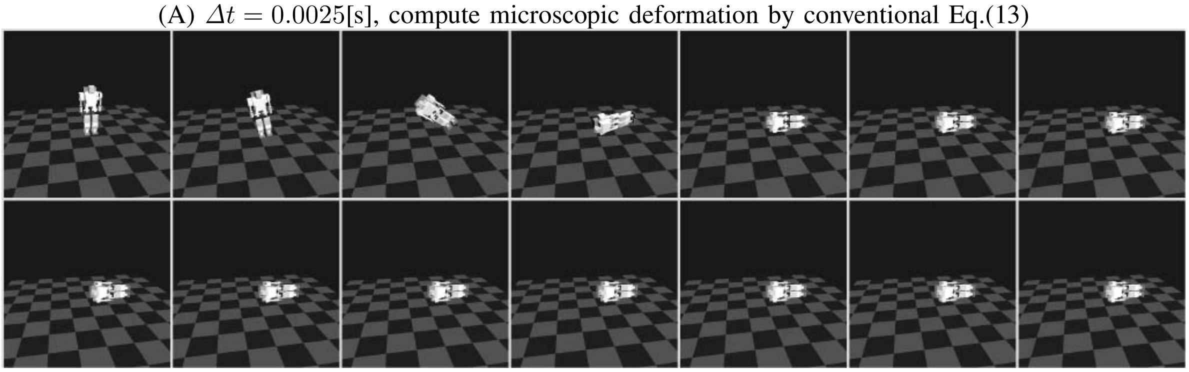

(B) $\Delta t = 0.0025$[s], compute microscopic deformation by proposed Eq.(14)

Fig. 6. Falling-down (and bouncing) motions of the robot to examine the proposed energy-suppression computation of micro-contact force

to the lack of reaction force for $\lambda \simeq 7.0$. Fig. 8 shows the distribution of reaction force to the vertices of the sole. They were disproportionate in terms of space for $\lambda = 0.01$, while smoothed for $\lambda = 4.0$.

D. Examination of static friction force

A walking motion was simulated on the floor model with $\lambda = 1.0$ (the other parameters were the same with that of section IV-C). And then, another floor model with maximum static friction coefficient 0 was also tested for the same motion. Δt was 0.001[s] for both cases. Fig. 9(A)(D) show the loci of COG of those motions with and without static friction, respectively. And, Fig. 9(B)(E) and Fig. 9(C)(F) are the loci of COG acceleration for the case with and without static friction, respectively. Though COG loci are similar to each other, the difference of them certainly appears in acceleration level. Namely, one can recognize the oscillation of the latter due to the dither of sole in tangential direction to the floor.

E. Other simulations

A success case of walking motion, a failure case, and a jumping motion were simulated as shown in Fig. 10, Fig. 11 and Fig. 12, respectively. For all of them, the floor was modeled as the same with in section IV-C($\lambda = 1.0$)

V. Conclusion

A fusion of micro/macro contact model was discussed in forward dynamics simulation of multibody system. A timestep-dependent variable damper introduced to the micro contact model basically avoids the oversupply of kinetic energy due to the quantized integration. And in the macro contact model, the time-space smoothing of reaction force was realized by error-norm minimization against a hyperstatistics problem.

References

[1] Brian Mirtich, John Canny. Impulse-based Simulation of Rigid Bodies. In *Symposium on Interactive 3D Graphics*, pages 181–188, 217, 1995.

[2] Scott McMillan and David E.Orin. Forward Dynamics of Multi-legged Vehicles Using the Composite Rigid Body Method. In *Proc. of the 1998 IEEE Int. Conf. on Robotics & Automation*, pages 464–470, 1998.

[3] Yoonkwon Hwang et al. An Order n Dynamic Simulator for a Humanoid Robot with a Virtual Spring-Damper Contact Model. In *Proc. of the 2003 IEEE Int. Conf. on Robotics & Automation*, pages 31–36, 2003.

[4] Katsu Yamane. *Simulating and Generating Motions of Human Figures*, volume 9 of *Springer Tracts in Advanced Robotics*. Springer-Verlag, 2004.

[5] K.H.Hunt and F.R.E.Crossley. Coefficient of Restitution Interpreted as Damping in Vibroimpact. *ASME Journal of Applied Mechanics*, pages 440–445, 1975.

[6] Duane W.Marhefka and David E.Orin. Simulation of Contact Using a Nonlinear Damping Model. In *Proc. of the 1996 IEEE Int. Conf. on Robotics & Automation*, pages 1662–1668, 1996.

[7] P.Lötstedt. Numerical Simulation of Time-Dependent Contact and Friction Problems in Rigid Body Mechanics. *SIAM Journal of Scientific and Statistical Computing*, 5(2):370–393, 1984.

[8] David Baraff. Fast Contact Force Computation for Nonpenetrating Rigid Bodies. In *Proc. on SIGGRAPH 94*, pages 23–34, 1994.

[9] Y. Fujimoto and A. Kawamura. Simulation of an Autonomous Biped Walking Robot Including Environmental Force Interaction. *IEEE Robotics & Automation Magazine*, 5(2):33–41, 1998.

[10] Wookho Son, Jeffrey C.Trinkle, and Nancy M.Amato. Hybrid Dynamic Simulation of Rigit-Body Contact with Coulomb Friction. In *Proc. of the 2001 IEEE Int. Conf. on Robotics & Automation*, pages 1376–1381, 2001.

[11] M. W. Walker and D. E. Orin. Efficient Dynamic Computer Simulation of Robotic Mechanisms. *Trans. of the ASME, Journal of Dynamic Systems, Measurement, and Control*, 104:205–211, 1982.

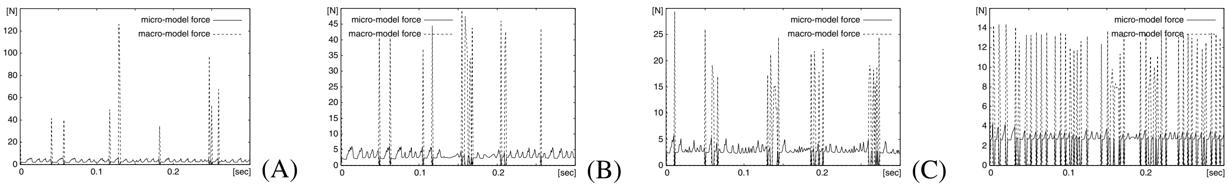

(A) $\lambda = 0.01$ (B) $\lambda = 0.1$ (C) $\lambda = 1.0$ (D) $\lambda = 4.0$

Fig. 7. Comparison of reaction force from the floor for λ in (33)

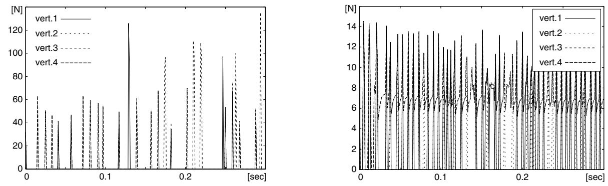

(A) $\lambda = 0.01$ (B) $\lambda = 4.0$

Fig. 8. Comparison of reaction force distribution to the contacting points for λ in (33)

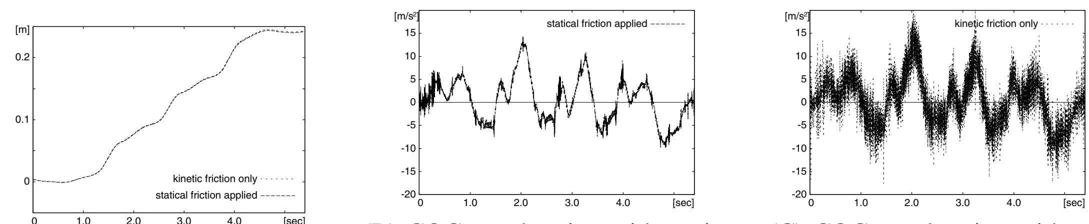

(A) COG locus along x axis (B) COG acceleration with static friction along x axis (C) COG acceleration without static friction along x axis

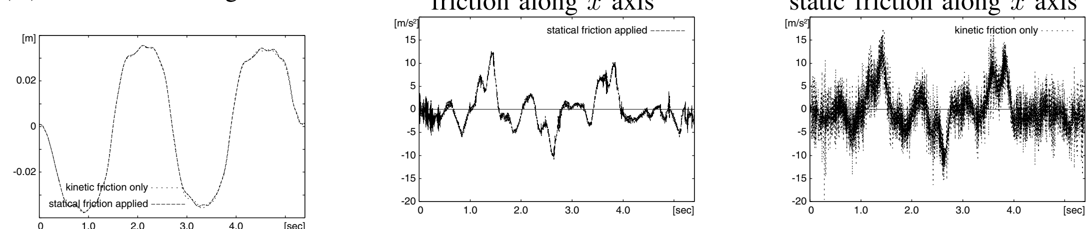

(D) COG locus along y axis (E) COG acceleration with static friction along y axis (F) COG acceleration without static friction along y axis

Fig. 9. COG loci of walking motions for friction force conditions

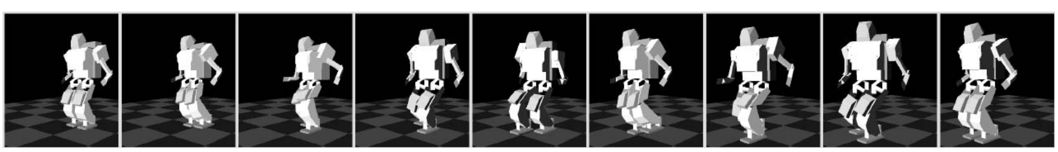

Fig. 10. Walking motion

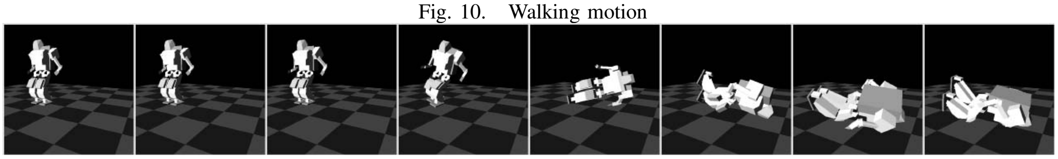

Fig. 11. Falling-down motion during a walking

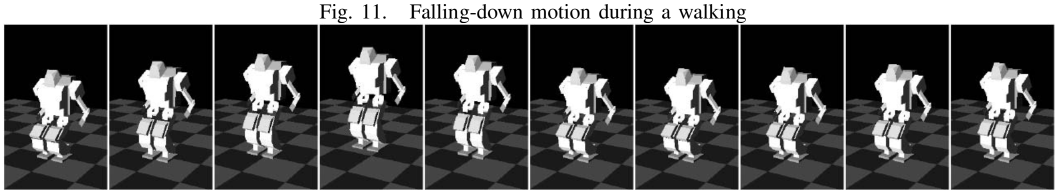

Fig. 12. Jumping motion

[12] A. Joukhadar, A. Deguet, and C. Laugier. A Collision Model for Rigid and Deformable Bodies. In *Proc. of the 1998 IEEE Int. Conf. on Robotics & Automation*, pages 982–988, 1998.

[13] http://www.automation.fujitsu.com/products/products07.html.